Available online at www.sciencedirect.com
ScienceDirect
International Journal of Solids and Structures 44 (2007) 5554–5575
INTERNATIONAL JOURNAL OF SOLIDS AND STRUCTURES
www.elsevier.com/locate/ijsolstr

Detecting damage through the processing of dynamic shapes measured by a PSD-triangular laser sensor

Bartolomeo Trentadue [a], Arcangelo Messina [b,*], Nicola Ivan Giannoccaro [b]

[a] *Dipartimento di Ingegneria Meccanica e Gestionale, Politecnico di Bari, 70126 Bari, Italy*
[b] *Dipartimento di Ingegneria dell'Innovazione, Università di Lecce, 73100 Lecce, Italy*

Received 4 May 2006; received in revised form 22 December 2006
Available online 23 January 2007

Abstract

There exist several studies in the literature which have shown the potentiality offered by certain vibration-based techniques aimed at detecting damage in structural systems. In all these existing techniques noise (distributed and/or outliers) plays a significant role and can make the difference between a successful or an unsuccessful application. In spite of such a mentioned remarkable influence, the studies aimed at investigating the influence of noise on the success of the techniques are not as rich in experimental details as they are in numerical simulations. In this work an extensive set of experiments aimed at evaluating the feasibility of certain diagnosing techniques is provided. This work should also be considered as the experimental validation of certain analytical and numerical simulations carried out in the past [Gentile, A., Messina, A., 2003. On the continuous wavelet transforms applied to discrete vibrational data for detecting open cracks in damaged beams. International Journal of Solids and Structures 40, 295–315; Messina, A., 2004. Detecting damage in beams through digital differentiator filters and continuous wavelet transforms. Journal of Sound and Vibration 272, 385–412] within the frame of real measurements based on a particular laser technology; in addition, the mentioned validating experiments illustrate certain peculiarities not shown in the past, and, finally, valuable benchmarks are provided for testing future diagnosing techniques in numerical simulations. The experimental set-up consists of both commercial and electronic circuits appropriately designed and realized, whose significance, in the measuring system is accurately described in order to increase the signal/noise ratio of the dynamical measurements.
© 2007 Elsevier Ltd. All rights reserved.

Keywords: Beams; Open cracks; Vibrations; Wavelets; Damage detection; Laser measurements

1. Introduction

Damage detection based on changes of modal data or, more in general, vibration-based data, has become one of the most attractive research topics in recent years (Dimarogonas, 1996; Salawu, 1997; Doebling et al., 1998).

* Corresponding author. Tel.: +39 0832 297 801; fax: +39 0832 297 733.
E-mail address: arcangelo.messina@unile.it (A. Messina).

0020-7683/$ - see front matter © 2007 Elsevier Ltd. All rights reserved.
doi:10.1016/j.ijsolstr.2007.01.018

A synthetic, but non-unique, classification, among the several proposals appeared in the literature, could be attempted by looking at techniques which are depending or non-depending models; the term *model* is referred to a mathematical model supporting the main features of the associated physical system under test (in this work also indicated with the acronym SUT). The mathematical model is often based on an updated or presumably reliable set of algebraic/differential equations through which a relevant response close to that of the real system is expected. The presence of uncertain boundary conditions, the complexity of the systems, the practical impossibility to get a full set of data can make the application of the depending model-based techniques non-straightforward or non-attractive from a practical point of view.

The present work is related to those methods that try to detect existence and location of damage through the processing of a dynamic shape strictly related to the SUT. Therefore, the diagnosing technique herein dealt with is a non-depending model. Certain *dynamical shapes* associated to damaged/undamaged transversally vibrating beams are measured and constitute the only information available to the analyst for carrying out a diagnosis on the state of health of the same beams. In this respect, the damage is simulated through a localized notch.

The simplicity of the physical model herein considered, *i.e.*, flexural vibrating beams, is taken into account, just like in the past investigations, only in order to focus the attention on the diagnosing techniques rather than on the complexity of the model. However it is believed by the authors that the relevant conclusions can be seen within a larger frame.

It is with respect to this particular structural element which since 1985 (Yuen, 1985; Pandey et al., 1991) have evidenced the possibility to extract diagnosing information through the analysis of the details in certain dynamical shapes. Since then, several techniques have been introduced in the literature, a part of which is mentioned in the references of works (Gentile and Messina, 2003; Messina, 2004). These references should not be considered exhaustive of all the existing techniques but well representative of a more extensive set. In particular, the review recently published by Kim and Melhem (2004) should also be taken into account in order to get an idea about the plentiful perspectives and NDE proposals for detecting damage in structural components by using wavelet analysis. Several proposals show advantages but very often are also accompanied by disadvantages and uncertainties which still leave scientific questions open. For example, Han et al. (2005) recently introduced wavelet packet based damage identification strategies for beam structures and, in spite of the admission of a certain potential of the method, they recognized that the need to resort to a reliable reference structural model in healthy (undamaged) conditions was an important limitation of the method. Kim et al. (2006) realized the importance of extracting (experimentally) reliable mode shapes on dense grids; these latter can be obtained by using a scanning laser vibrometer (Pai and Young, 2001; Waldron et al., 2002; Chukwujekwu Okafor and Dutta, 2000). A part from the particular suggested techniques, the literature has recently shown a certain convergence of opinions on the importance to have available reliable measurement set-ups along with a huge number of measured points.

This work is specifically interested in the derivatives of dynamical shapes which, in principle, are able tools for identifying local damage without resorting to information related to the system in the undamaged or previous conditions. In this respect, Messina (2004) illustrates an accurate review on the subject and a close correlation between the derivatives, differentiator filters and continuous wavelet transforms. In order to avoid redundancy, the introductive material illustrated in reference (Messina, 2004) is considered part of the present work. Here it is finally worth mentioning recent findings by Rucka and Wilde (2006) which extended relevant ideas of continuous wavelet transforms from damaged beams to damaged plates.

This work, apart from the introductive and conclusive sections, is divided into three main parts. The first part illustrates the SUT, its related experimental set-up and the analytical method herein used in order to experimentally estimate the related dynamical shapes. The second part illustrates a set of measurements related to a specific undamaged beam; in this second part an error/noise analysis, concerned with the signal/noise ratio of the extracted dynamical shapes is also carried out and the limits related to the particular laser technology used are elucidated. The related sections are enriched in experimental details which clarify the reasons involving measurement errors, thus the importance of having available good quality measurements gives the problem we have dealing with its right dignity. Finally, the third part illustrates a set of measurements carried out on several types of beams having different geometric and material characteristics; in this section interesting valuable peculiarities are elucidated, and recommended for diagnosing purposes.

All the experimental tests are based on measuring a highly redundant number of points (a few hundreds) in order to completely validate the past conclusions (Gentile and Messina, 2003; Messina, 2004) which pioneered the case from a numerical point of view.

The detailed description of the measuring system, finally, permits the extraction benchmarks of signal/noise ratios which should be necessarily considered in numerical simulations for future proposals. In this respect, the richness of experimental details herein reported suggests that the mentioned technique could not be suitable in a black box-sense, but needs skilled operators who would be able to bring together numerical processing and electronic measuring system knowledge. In particular, electronic measuring systems (comprising the most recent laser systems) should not be used in a black box sense because any apparently small detail is an important step forward in increasing the signal/noise ratio and thus, making the difference between a successful or an unsuccessful damage detection procedure. Finally it is believed that all findings herein illustrated are applicable in all structures where, independently from whether it is visitable or not, allow a multi-grid measurability.

2. The physical model and its experimental set-up

The system taken into account in the present work is schematically shown in Figs. 1–3. In particular, Fig. 1 illustrates a plan of the whole mechanical assembly of the system under test (SUT) whilst Fig. 2 shows its physical realization. As far as the electric links of the electronic devices used in the experimental set-up are concerned, Fig. 3 should be taken into account.

2.1. The SUT: mechanical part

The system under test consists of a clamped-free beam. Based on Fig. 1, the beam is clamped through a vice rigidly screwed onto the top of a laboratory table; this table, indicated as ground 2, is characterized by the first resonance, for an in-plane (parallel to the supporting top) mode shape, of about 500 Hz; the same table supports a small electromagnetic shaker (sine rated peak force 9 N; working in a frequency range 2–11 kHz with a maximum travel and acceleration of 3 mm and 61×9.81 m/s^2, respectively). The experimental arrangement is such that the beam undergoes transversal vibrations as shown in Fig. 1. Such vibrations are essentially sinusoidal. In order to measure point-by-point the peak displacements of the beam, a laser sensor head longitudinally moves in front of the beam; the apparatus supporting the laser sensor belongs to another ground (called ground 1 in Fig. 1) which essentially is another table placed in front of ground 2 (Fig. 2). The floor

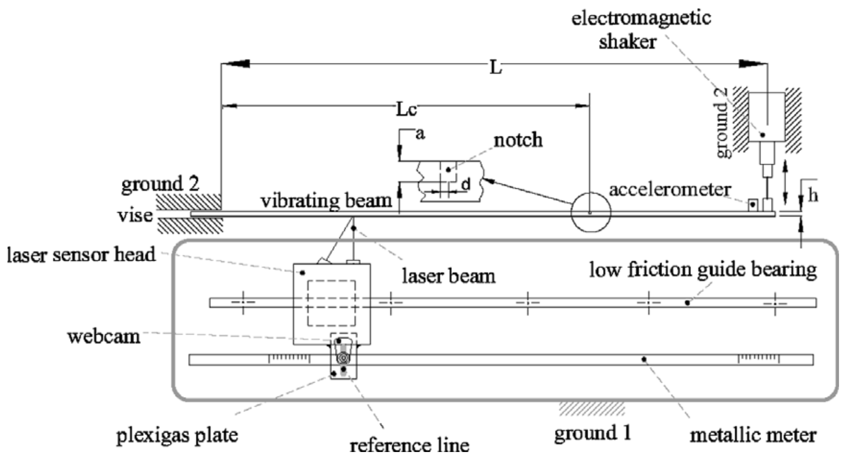

Fig. 1. Plan of the mechanical arrangement concerning the system under test.

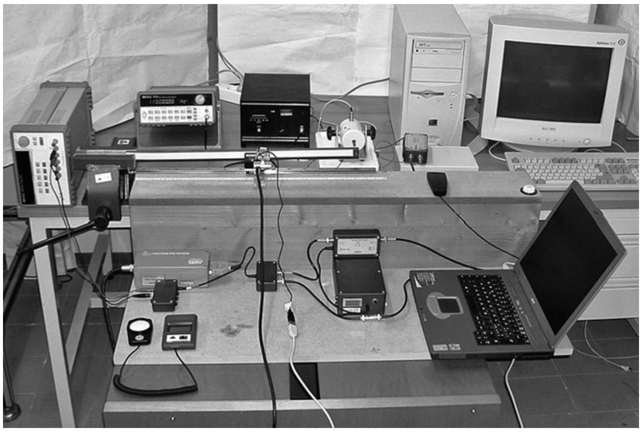

Fig. 2. Photograph of the whole experimental setup.

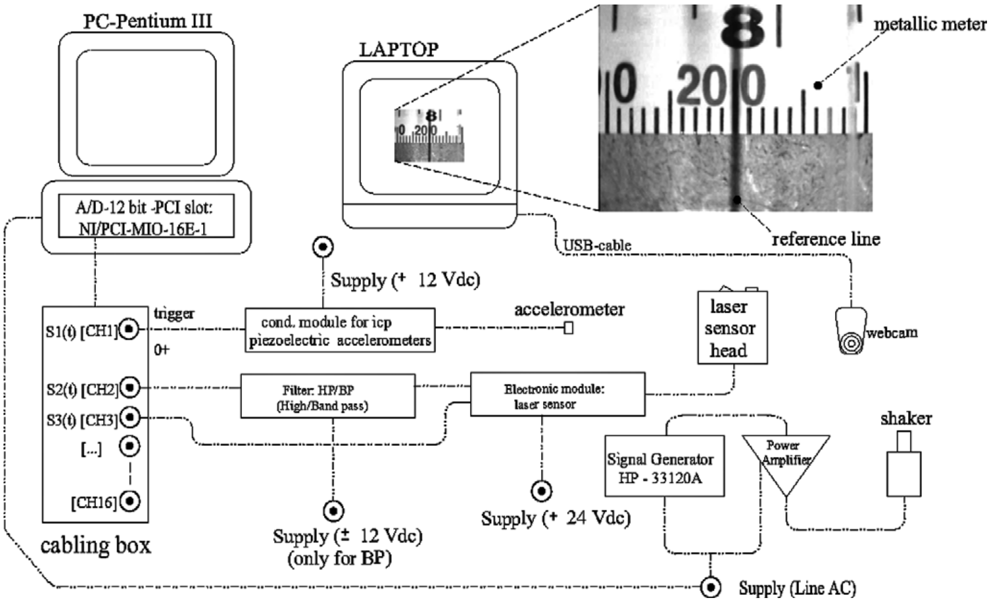

Fig. 3. Links of the electronic arrangement concerning the system under test.

supporting both the grounds constitutes a natural mechanical decoupling in order to avoid appreciable transmission of the vibrations from the shaker to the laser sensor.

The laser sensor head is manually moved point-by-point by sliding over an NSK low friction guide bearing; the sensor is mechanically mounted through an aluminium plate onto the trolley of the guide. In order to give an appreciably good position of the sensor along the beam a metallic meter is glued parallel to the guide bearing whilst a red reference line is drawn on a plexigas (transparent) plate; this latter is rigidly glued to the aluminium plate, moves rigidly with the laser sensor head and overlaps the metallic meter. However, if the visual inspection is used to evaluate the position of the laser sensor head around a millimetre line, the estimation can contain parallax errors depending on the relative positions of *eyes*, *reference line* and *metallic meter*. Based on a rule of thumb, the experimental arrangement used in this work caused parallax errors even of ±250 μm. Therefore, in order to reduce the inaccuracy concerning the identification of the position, a webcam was fixed onto the top of the laser sensor head by placing the relevant objective at a few centimetres from the reference line. The image, which was sent to a laptop (Fig. 3), allowed a very accurate visual estimation of the position of the laser head sensor. All the measurements were so established with a density of 1 point/mm.

2.2. The SUT: electronic part

The laser sensor herein used is based on PSD-triangular technology and essentially measures distances (MEL Mikroelektronik GMBH, 2002); it must be placed with its objective, perpendicularly to the tested surface, at a stand-off distance of 24 mm (zero baseline distance); the measurable displacement range around the stand-off distance is ±2 mm with a resolution of 1 μm. The output of the laser sensor head is conditioned by an electronic module which provides an analog output voltage signal in the range ±10 V through a low impedance output (<0.1 Ω). The technical specifications provided by the supplier have permitted to obtain (based on a standard linear fitting procedure) the following linear relation (1) between the output voltage and the measured distance.

$$y_{[\mathrm{mm}]} = -24.0001 + 0.200267 y_{[\mathrm{V}]}. \tag{1}$$

The displacement of the point taken into account is indicated as y whilst the measured and/or converted physical magnitudes are indicated in squared brackets. For the sake of generality, all the measurements will be shown in electric dimensions [V]; the mechanical magnitudes can be obtained through Eq. (1).

The apparatus constituted by both the laser sensor head and the electronic module is characterized by a low-pass type frequency response function having a −3 dB frequency placed at about 10 kHz and to which 0.1 ms of integration time corresponds. Dip switches inside the electronic module enable higher integration times (causing a lower −3 dB frequency) to which corresponds a lower level of emitted noise. In this respect, in all the following measurements 2 ms (being the consequent −3 dB frequency equal to 250 Hz) was selected.

As is illustrated in Fig. 3, the signal ($y_{[\mathrm{V}]}$) coming out from the electronic module feeds a filter ($S_2(t)$): this is a band pass, a high pass or none filter depending on the relevant case studied. The high pass filter is simply based on a classical CR-network ($C = 22nF$; $R = 1$ MΩ) whilst the band pass filter is an analog active circuit (Messina, 2005) presenting a particularly narrow band around the relevant frequency of the signal; its band can be selected by changing a few discrete components on the printed circuit board. Such a pass-band filter is essentially built by cascading three second order stages which allow two global −3 dB points at ±5 Hz around the central frequency. The input and output stages of such an analog filter are complemented through two single-ended buffers; the noise emitted, with respect to a 50 Ω-input, is 50 μV_{rms} (estimation through a 400FL-AC Hewlett Packard voltmeter in its 4 MHz passing band). From the electronic module a signal (0–10 V), representing the reflected light during the operation of the laser sensor head ($S_3(t)$), is also measured: this signal provides an idea of the stability and quality of the measured vibration at the point of interest (MEL Mikroelektronik GMBH, 2002). This signal was not filtered because it was not directly of interest in the post-processing stage.

In Fig. 3 an ICP-accelerometer which is placed in a fixed position of the vibrating beam (Fig. 1) for all the tested points and whose relevant conditioned signal is $S_1(t)$ is also shown. The presence of this accelerometer provides the time reference for extracting the phase, thus allowing the extraction of the relevant mode shape (essentially the negative and positive parts of the mode shapes).

In all the measurements illustrated in this paper, the bits of the 12 bit-A/D converter were employed in the following voltage ranges: [±2.5 V], [±5.0 V], [±10 V] for the signals S_1, S_2 and S_3, respectively.

Based on Fig. 3, the signal generator establishes a sinusoidal signal which is sent to the power amplifier; the frequency of this signal is close to a resonance of the beam. The power amplifier provides the appropriate power to the shaker which induces a steady-state of vibrations on the beam; in settled circumstances the relevant mode shape is dominant. The beam is characterized by approximately clamped-free ends and its resonances can be estimated basing the calculations on a classical Euler–Bernoulli beam model (*e.g.*, Rao, 1995). The frequency of the sinusoidal signal was established by tuning the signal generator through the relevant knob and hearing/comparing the resonance condition to the estimated ones. As it is well known (*e.g.*, Heylen et al., 2003; Ewins, 1992) this is not the only way to identify the resonance frequencies. However, in this work the technique employed aimed at extracting mode shapes is not the main objective; moreover, it is believed that the mentioned technique is an attractive practice founded on its simplicity; finally this way to identify the resonances, as shown in the next measurements, does not compromise the diagnosing technique and, therefore, this could also be considered interesting from a practical point of view.

Once the system vibrated in its steady-state, the operator moved the laser sensor head mm-by-mm in order to acquire sampled displacement data; each single operation was carried out by simply pushing an on/off switch (not shown in Fig. 3 for the sake of brevity) linked to a digital input of the A/D PCI-board (DIO0). A code written in MATLAB(R14)/C allowed an automatic saving-operation for each point-by-point measurement. Although the electronic system allowed such a mentioned automatic measuring process, the process in total took about 5–6 h for a skilled operator over a number of 450–550 measured points.

2.3. The method used to experimentally estimate the dynamical shapes of the SUT

Based on the fact that the beam is excited by a sinusoidal force close to a resonance frequency (say kth) and due to the decoupling of the resonance frequencies of the particular SUT, it is expected that each point vibrates in a sinusoidal regime with a dominance of the kth mode. Therefore, the fitting procedure has been based on the minimization of the error (e_j) shown in Eq. (2)

$$e_j = \sum_{i=1}^{N} (y_i - M_j - A_j \cdot \sin(\omega_k \cdot t_i) - B_j \cdot \cos(\omega_k \cdot t_i))^2 \quad \text{for } j = 1, \ldots n. \tag{2}$$

In Eq. (2) y_i is the ith sampled measured sinusoidal displacement; the minimization of e_j is aimed at providing three parameters (M_j, A_j, B_j) which, algebraically composed, yield the amplitude $((A_j^2 + B_j^2)^{1/2})$ and the phase (respect to the fixed accelerometer) in the jth point of the beam. Indeed, these three parameters are the only unknowns in Eq. (2): N refers to the number of settled samples in time domain for each established jth position whilst ω_k refers to the exciting frequency established by the signal generator. In order to seek a simpler nomenclature, the index j will not be shown in the next equations.

The above mentioned three parameters (M,A,B) in (2) can be evaluated through three necessary conditions obtained by equating to zero the first partial derivative of the error e with respect to the parameters ($\partial e/M,A,B = 0$). Such three conditions yield the following linear and symmetric system (3)

$$\begin{bmatrix} N & \sum_{i=1}^{N} \sin(\omega_k \cdot t_i) & \sum_{i=1}^{N} \cos(\omega_k \cdot t_i) \\ & \sum_{i=1}^{N} \sin(\omega_k \cdot t_i)^2 & \sum_{i=1}^{N} \sin(\omega_k \cdot t_i) \cdot \cos(\omega_k \cdot t_i) \\ \text{sym} & & \sum_{i=1}^{N} \cos(\omega_k \cdot t_i)^2 \end{bmatrix} \cdot \begin{pmatrix} M \\ A \\ B \end{pmatrix} = \begin{pmatrix} \sum_{i=1}^{N} y_i \\ \sum_{i=1}^{N} \cdot y_i \sin(\omega_k \cdot t_i) \\ \sum_{i=1}^{N} \cdot y_i \cos(\omega_k \cdot t_i) \end{pmatrix}. \tag{3}$$

The solution of this system provides the parameters (M,A,B). It is interesting to notice that Eq. (3) can even be simplified if the samples are appropriately sampled in an integer number of periods. In such a situation, indeed, the off diagonal terms of the matrix coefficients would be nullified, M would reduce to the mean value of the sinusoidal law in the time domain and, finally, (A,B) could be obtained by solving a diagonal system of two linear algebraic equations after having removed the mean. The described simplification was followed in the present work. However, it could be of interest to know that along with the mentioned simplification, a practice was also followed to reduce the leakage effect. In this latter respect, it should be taken into account that the sampling frequency can be settled only in a finite and discrete way depending on the A/D converter adopted and on the selected number of channels; on the other hand, ω_k depends on the SUT; therefore in order to get an integer number of periods and a reduced leakage phenomenon an appropriate sampling frequency should be adopted among the available ones by the A/D.

It is finally stressed that the submitted work does not measure, in a strict sense, *mode shapes* but *dynamic shapes*. In particular, no modal analysis is carried out for extracting complex mode shapes; rather, the amplitude of the vibration is measured when the frequency of a sinusoidal excitation is close to the relevant resonance of the structure. This is also accomplished through the presence of a narrow analog pass-band filter in order to reduce extraneous contributions. In such a way the experimental measurements consist directly of measuring real data and no numerical process, aimed at separating real parts from complex ones, is taken into account.

3. Measurements of undamaged beams and error analysis

It should generally be accepted that the identification of a notch in a beam heavily depends on the signal-noise ratio. The dependence of the signal/noise ratio on the involved several factors is, therefore, elucidated in this section.

The tests have been carried out on the second mode shape of an aluminium beam whose geometric and structural characteristics are referred to as beam1 in Table 1. Table 1 also illustrates all the beams investigated in this work.

Based on the experimental setup discussed in Section 2 several measurements point-by-point were carried out in order to identify those factors which could improve or degrade the quality of the measurement regarding a mode shape. To this end, the experience conducted by the authors yielded to consider as mainly significant the experimental scenarios described in Table 2.

As is clear from Table 2, the acronyms are related to the particular scenario through the binary index 1/0 which means whether each single condition exists or not, respectively; the last letter d/s indicates a dynamic/static measurement, respectively. In this latter respect, it should be considered that in a dynamic measurement the mode shape is estimated as discussed in Section 2.3 whilst in the static case the measurement corresponds to a static deflection evaluated by averaging the samples in time domain when the laser sensor head was placed at fixed points along the beam.

Table 1
Geometric and material characteristics of the beams under test

Ref.	Material description	Length L (mm)	Thickness h (mm)	Width b (mm)	Young's modules E (GPa)	Density ρ (kg/m^3)	Frequency[b] second mode (Hz)
Beam1	Aluminium alloy	588	3.4	25.4	75	2400	56
Beam2	Plastic laminate	570	16	20	6.9[a]	1360[a]	110
Beam3	Epoxy glass laminate	500	5	20	12.4[a]	1900[a]	66
Beam4	Epoxy glass laminate	500	10	20	12.4[a]	1900[a]	113

[a] Declared by the supplier.
[b] Estimated by manual sine-sweep in undamaged (beam1) and damaged (beam2,3,4) conditions and mechanically arranged as in Fig. 1.

Table 2
Experimental scenarios aimed at estimating the second mode shape of beam1

Acronim scenario	Scenario description
$F_1D_1T_1$d	Filter placed downstream the electronic module: band pass; measurements carried out in Dark conditions (averaged illuminance[a] = 23 lx); white Tape glued along the beam; dynamic measurement
$F_1D_1T_0$d	Filter placed downstream the electronic module: band pass; measurements carried out in Dark conditions (averaged illuminance[a] = 24 lx); Tape absent, shiny surface; dynamic measurement
$F_1D_0T_1$d	Filter placed downstream the electronic module: band pass; measurements do not carried out in Dark conditions (averaged illuminance[a] = 320 lx); white Tape glued along the beam; dynamic measurement
$F_0D_1T_1$d	Filter placed downstream the electronic module: high pass made of passive elements (R,C); measurements carried out in Dark conditions (averaged illuminance[a] = 27 lx); white Tape glued along the beam; dynamic measurement
$F_0D_1T_1$s	Filter placed downstream the electronic module: none; measurements carried out in Dark conditions (averaged illuminance[a] = 27 lx); white Tape glued along the beam; static measurement

[a] An ISO-TECH ILM 350 luxmeter was placed at mid span of the beam; the illuminance was measured by orienting the sensor in the canonical spatial directions and averaged.

In all the measurements concerning this and the next sections, point no. 1 was placed at about 44 mm from the clamped section of the beam shown in Fig. 1. It should be considered that for practical reasons concerning the mutual positioning of both the grounds and occurring test-by-test, a slight change in the number of the points has to be expected; this however, is not a serious drawback when interpreting the experimental measurements. Finally, it is stressed that, unless differently specified, the signal/noise ratio is intended as the magnitude evaluated by Eq. (4)

$$s/n = 20\log_{10}(y_{\max}/\sigma). \tag{4}$$

The parameter σ represents the standard deviation of the noise overlapped to the measurement whilst $y_{\max}$ is the absolute maximum displacement of the dynamical shape. The standard deviation (σ) is estimated by carrying out a polynomial fit over the point-by-point measurements and evaluating the standard deviation of the residues.

The A/D conversion regarding the tested points of beam1 was based on a sampling frequency of 144.927 kHz by sampling 25,880 samples in the range of 10 periods of a sinusoidal signal having a frequency of 56 Hz (Table 1). Eqs. (3) were, therefore, applied, period-by-period averaging the magnitudes on the ten acquired periods for each point fixed along the space of beam1. In total, the dynamic shape concerning beam1 was evaluated over 544 points.

3.1. Influence of the reflecting surface

Based on the previously mentioned scenarios the dependence of the signal/noise ratio from the reflecting surface is taken into account here. In this respect Figs. 4a and b illustrate the sinusoidal measurement carried out in point no 544 referred to the corresponding scenarios $F_1D_1T_1d$ and $F_1D_1T_0d$, respectively. Both Figs. 4a and b illustrate three sampled magnitudes ($S_1(t)$, $S_2(t)$, $S_3(t)$ as described in Fig. 3) in Volt. The approximately constant voltages of Fig. 4 correspond to $S_3(t)$: *i.e.*, the reflected light of the laser sensor head; the continuous sinusoidal line (amplitude: ~5 V) is the signal coming from the laser sensor head ($S_2(t)$) and, finally the dashed sinusoidal line (amplitude: ~1 V) corresponds to the conditioned signal of the accelerometer ($S_1(t)$). The comparison between Figs. 4a and b clearly illustrates how the absence of a tape can cause a more unstable signal for the reflected light ($S_3(t)$). Although both of the figures illustrate a smooth measurement of $S_2(t)$, an extensive set of experiments showed a heavy overall effect on the measured points yielding a poor signal/noise ratio for the estimated mode shape. In order to corroborate this aforementioned conclusion Fig. 5 illustrates the second mode shape measured over a total of 544 points for $F_1D_1T_1d$ (a) and $F_1D_1T_0d$ (b), respectively. In particular, the graphs on the top of Fig. 5 also shows a polynomial fit of the mode by using polynomials of order $p = 8$; the fitting curves are slightly shifted down for the sake of clarity; the residual noise, obtained by the difference between the original data and its related fit is displayed at the bottom of each relevant picture.

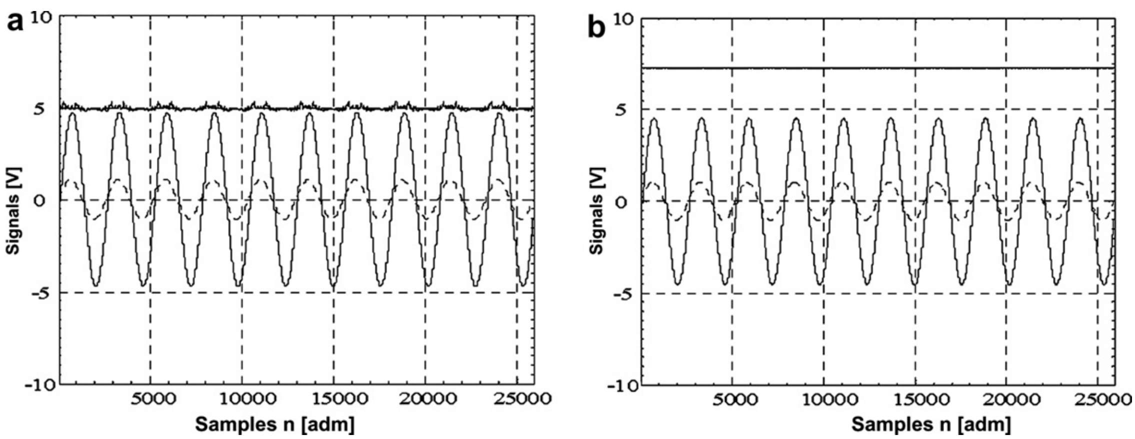

Fig. 4. Sinusoidal vibration at free edge of an undamaged aluminium beam without (a) and with (b) the interposition of white tape.

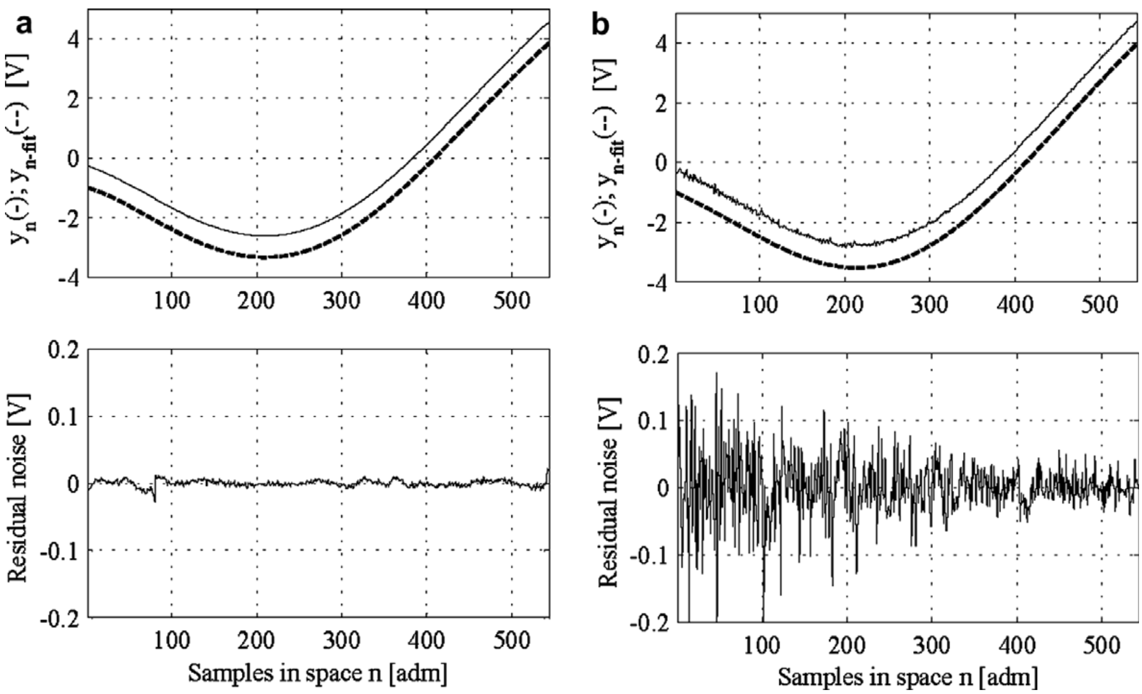

Fig. 5. Overall effect of the presence (a: $p = 8$) and absence (b: $p = 8$) of white tape on the signal/noise ratio of dynamic measured shapes.

The comparison between Figs. 5a and b clearly shows the superiority of the measurement when the shine of the surface is reduced through the interposition of the white tape. In order to provide numerical benchmarks, Table 3 lists the relevant signal noise ratios associated to the measurements illustrated in Fig. 5 based on different orders of polynomial fittings.

A perusal of Table 3 reveals how the standard deviation of the noise contained in the mode shape is about 1 order of magnitude higher than measurements made without making opaque the surface. On the other hand Table 3 clarifies that there exists the possibility to extract mode shapes which have an appreciable high signal/noise ratio even by using a simple extracting method as that which this paper is dealing with. Finally, it is interesting to notice how the increasing order of the polynomial fitting seems to be asymptotically stable. However, in all the following measurements an order of 8 for the polynomial curve fitter is taken into account for discussions related to the signal/noise ratios.

Fig. 6 is provided in an attempt aimed at illustrating the shine of beam1 whilst Fig. 7 shows the several beams subjected to the tests by using the white tape on the interested surfaces.

3.2. Influence of illuminance and analog filters

In this subsection the dependence of the signal/noise ratio on the illuminance and on the presence of particular analog filters is taken into account. In this respect, Table 4 illustrates, similarly to Table 3, the standard

Table 3
Numerical benchmarks for the signal/noise ratios associated to beam1: shine

Order of polynomial fitting (p)	$F_1D_1T_1d$		$F_1D_1T_0d$	
	σ (mV)	s/n (dB)	σ (mV)	s/n (dB)
5	6.59	56.8	47.67	39.9
8	5.04	59.1	45.91	40.3
12	4.12	60.8	45.63	40.3
18	3.99	61.1	45.37	40.4

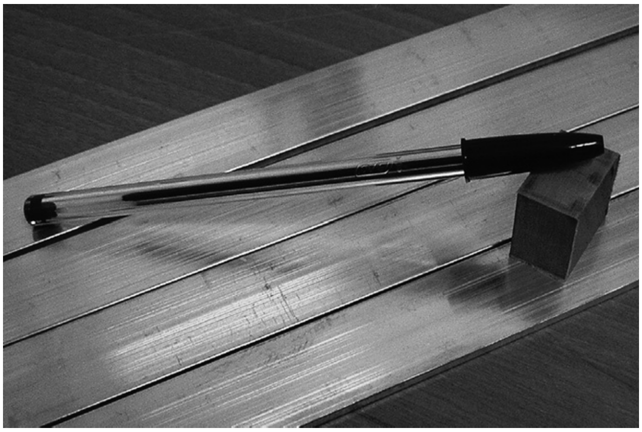

Fig. 6. Shine of the aluminium beams under test.

Fig. 7. The beams under test. From top to bottom: beam1, beam3, beam4, and beam2.

Table 4
Numerical benchmarks for the signal/noise ratios associated to beam1: illuminance and filters

Order of polynomial fitting (p)	$F_1D_0T_1d$		$F_0D_1T_1d$	
	σ (mV)	s/n (dB)	σ (mV)	s/n (dB)
5	8.65	53.5	7.48	53.6
8	4.47	59.2	3.06	61.3
12	4.37	59.4	2.81	62.1
18	4.20	59.7	2.69	62.5

deviations and the signal/noise ratios along with the increasing order of the polynomial curve fitter. This performance is also illustrated in Fig. 8 where, based on the same previous conventional graphical representation, Figs. 8a and b refer to $F_0D_1T_1d$ and $F_1D_0T_1d$, respectively when the 8th order of the curve fitter is taken into account.

Apart from the occurring outliers, the standard deviations do not seem particularly influenced by the illuminance or by the presence of a band or high pass filter. In all the cases investigated in Table 4 the signal/noise ratio is higher than 50 dB and the standard deviation of the noise extracted from the mode shape is about

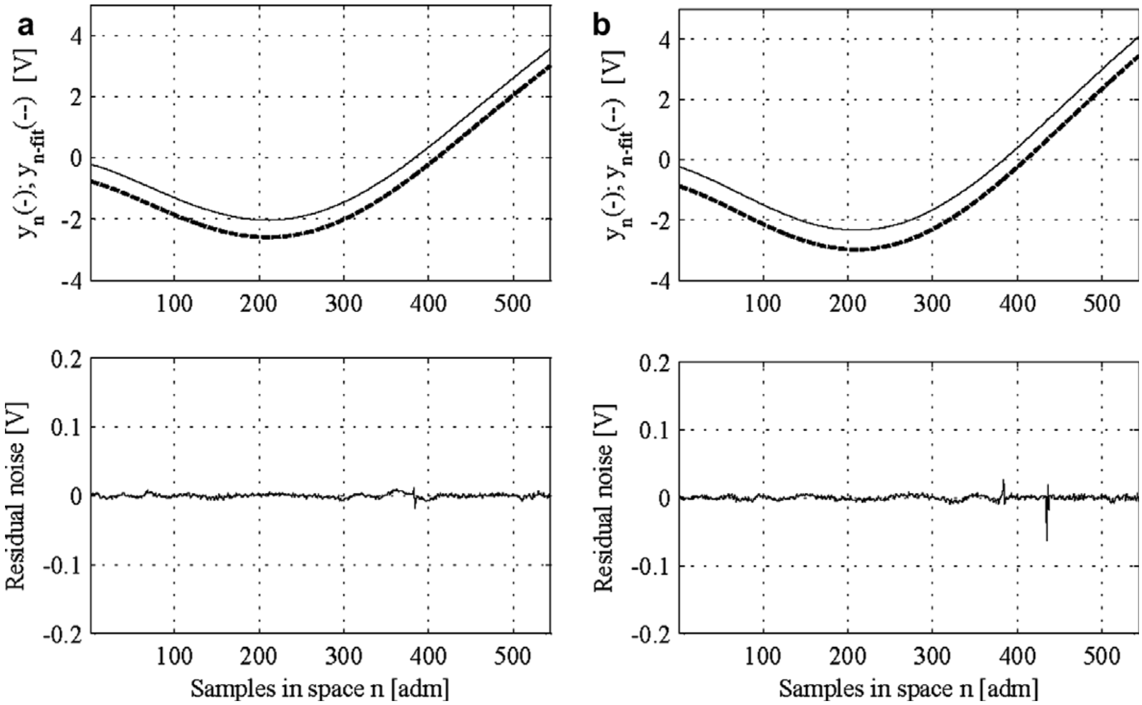

Fig. 8. Dynamic shapes measured by using passive high pass filter (a: $p = 8$) and active band pass filter (b: $p = 8$).

4 mV. In this respect Tables 3 and 4 prove an excellent repeatability of the experimental set-up used. What can possibly be argued is whether a better performance exists when the active band pass filter is substituted by the passive high pass one; indeed, in this latter case Table 4 shows a very low standard deviation of the extracted noise; however, in spite of this attractive performance, the choice of using a passive high pass filter should be taken into account when the analyst aims at carrying out the sampling process without preventing possible aliasing. For this reason and based on the very slight difference related to the presence or absence of the active band pass filter, all the following measurements are based on condition F_1.

3.3. Suitability of static measurements

In order to show whether the choice of an analyst, aimed at carrying out a diagnosing procedure, is in practice equivalent between a static or dynamic shape, this case has also been investigated. For this, with a view to using derivatives of shapes in order to detect the presence of possible cracks, a static deflection shape is in theory equivalent to a dynamic shape. However, Figs. 8 and 9 show how such a theoretical principle can be violated in practice. In particular, the graph at the top of Fig. 9 shows the measure of beam1 when it is placed in its quiet condition. The presence of the curvature is justified by the fact that beam1 is not exactly a straight beam but it presents an initial slight curvature. The presence of an initial curvature is not believed to be a serious drawback; conversely the serious limitation is due to the fact that the operation aimed at measuring a static deflection also includes the superficial irregularities which can yield a non-negligible amount of noise. Indeed, the graph at the bottom of Fig. 9 and Table 5 illustrate a non-negligible amount of noise (about 30 mV: corresponding to 6 μm by Eq. (1)). What should be considered remarkable in this discussion is the fact that the beam, whose static measurement is depicted in Fig. 9 (beam1), is the same beam which has a dynamic deflection such as that illustrated in Figs. 5 and 8. The absence of the superficial irregularities in a dynamic shape is due to the fact that the electronic setup of Fig. 3 eliminates point-by-point the dc-component (both the band pass or high pass filter analogically exclude the dc-component from $S_3(t)$) and, therefore, the estimated dynamic amplitude only depends on the global stiffness of the beam. In these circumstances, the magnitude

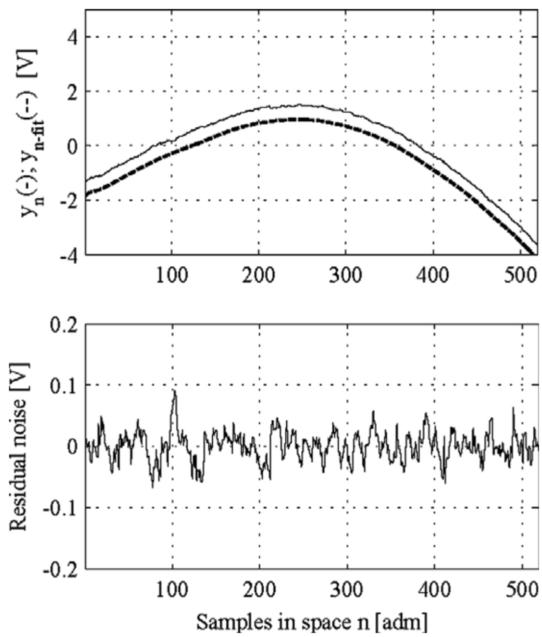

Fig. 9. Static measurement based on condition $F_0D_1T_1s$ (ref. Table 2) and $p = 8$.

Table 5
Numerical benchmarks for the signal/noise ratios associated to beam1: static measurement

Order of polynomial fitting (p)	$F_0D_1T_1s$	
	σ (mV)	s/n[a] (dB)
5	31.94	41.2
8	28.16	42.3
12	25.19	43.2
18	24.06	43.6

[a] Evaluated through y_{max} after removing the mean.

of the micro-irregularities cannot influence the dynamic response of the beam and, therefore, the result is a smooth response (Figs. 5 and 8). In a nutshell, the dynamic shape is a natural mechanical filter which avoids measuring the superficial irregularities.

In conclusion and in practice, a dynamic shape is believed to be more suitable than a static deflection shape. In passing, it should also be considered that the analyst has virtually many dynamic deflection shapes available which depend on the sensitivity of its measuring system.

3.4. Concluding benchmarks

In this section an extensive experimental investigation is presented; the experimental analysis of the errors has yielded the result that the noise contained in the dynamic shapes can be contained in the range of a standard deviation with a signal/noise ratio of about 50 dB. The outliers can occur around points where phase changes and in unknown circumstances. The noise estimated in this work is, however, in line with the benchmarks adopted in references (Gentile and Messina, 2003; Messina, 2004) and the relevant results can therefore be considered to be experimentally validated. It is finally added that such benchmark figures have been insulated in a laboratory environment where the dynamic shapes have been extracted by a simple PSD laser sensor technology through a simple experimental set-up. The investigations carried out have also provided guidelines for carrying out measurements which have a signal/noise ratio of 50 dB based on the laser technology adopted. Based on the nomenclature adopted since Table 2, all the following measurements will be carried out on condition $F_1D_1T_1d$.

4. Measurements of damaged beams and theoretical justifications

Within the frame of classical beams in bending conditions, the curvature $\chi(x)$ can be related to the bending moment $M(x)$ and to the bending stiffness $E(x)J(x)$ as in (5)

$$\chi(x) = \frac{M(x)}{E(x) \cdot J(x)}. \tag{5}$$

Based on Eq. (5) Pandey et al. (1991) illustrated the capability of the second derivative of a mode shape to locate damage on a beam. Such a capability can be related directly to the continuity of the bending moment through the length of the beam. Indeed, because of the presence of a continuous bending moment $M(x)$, whatever the distributed static or inertial dynamical load, a local change in the bending stiffness (EJ) is locally revealed through Eq. (5).

Eq. (5) also provides the tool to carry out a analysis of sensitivity aimed at identifying the most sensitive location for the kth mode. The answer should be related to the principle that, for an established kth mode, a certain location is considered more sensitive than another when the peak of the first is higher than that of the second location; more specifically, the height of the local peak should be intended with respect to the smooth (*i.e.*, undamaged) curvature in the proximity of the damaged location.

Based on the above mentioned principle, Eq. (5) is able to show that the location where the kth mode could better show the presence of damage corresponds to the location where in undamaged conditions the absolute curvature is maximum. Conversely, damaged locations occurring near to low values of curvature can be poorly identified. This naturally suggests that several modes or dynamical shapes should be used to identify a local damage and, possibly, all those occurring in the measurable range of frequencies.

If Eq. (5) can clearly illustrate the dependence of the sensitivity of the second derivatives with respect to the curvature, the dependence of the amount of damage with respect to the inherent characteristics of the beam it is less obvious. In a nutshell, an analysis aimed at estimating the minimum detectable amount of damage (*e.g.*, a/h in Fig. 1) with respect to the characteristics of the beam does not seem obvious, and, in particular, it is even worse in the presence of experimental noise. In this respect, the following experimental tests are, therefore, also aimed at testing whether the depth of a crack is independent from the characteristics of a beam. It will be shown that the capability of the second derivatives to identify an established amount of damage (intended as established $a/h = 0.5$ in Fig. 1) *depends on the particular beam under test*.

Therefore, what the following experiments are going to illustrate is not only a valuable validation of previous investigations (Gentile and Messina, 2003; Messina, 2004); rather, it also consists of proving that an identical a/h can be identified with a different sensitivity depending on: (i) the structure, (ii) the amount of noise contained in the measurements, (iii) the location of the damage in the relevant dynamical shape.

In order to pursue the above mentioned objectives, all the following experimental tests are characterized by the geometric characteristics listed in Table 6. The table also reports the details concerning the sampling process carried out point-by-point along the beam. As can be seen in Table 6, the depth (a/h) and the width (d) of the crack is constant for all the analyzed beams. Moreover, the location of the crack (Lc in Fig. 1) is geometrically different but *modally* constant for all the beams; indeed, based on the different length of the beams $Lc = 0.53L$ which corresponds to the internal point of a clamped-free beam where the curvature of the second mode shape is maximum. In this respect, the second mode was used to make all the discussed cases comparable; therefore, the use of the second mode should not be intended as exclusive for the adopted technique but only dictated by the need for comparison. The sampling frequency and the number of samples have been settled as discussed in Sections 2.3 and 3.

Finally, in order to challenge the noise contained in the measurements and simultaneously estimate the numerical second derivative of the signal (dynamic shape in space domain), the following convolving discrete sequence $h(n)$ has been adopted (Messina, 2004) in this work through the samples placed along the beams.

Table 6
Geometric and characteristics of the beams under test and electronic set-up

	Crack location Lc (mm)	Crack width d (mm)	Crack depth a/h	Sampling frequency (kHz) for each point along the beam	Samples in time for each point along the beam	Samples along the beam (N)[a]
Beam1	311	1.0	0.5	144.93	25,880	~540
Beam2	302	1.0	0.5	158.73	14,300	~520
Beam3	265	1.0	0.5	158.73	24,050	~450
Beam4	265	1.0	0.5	166.68	14,750	~450

Average illuminance = 30 lx, $F_1D_1T_1d$ (ref. Table 1).
[a] The number of points along the beam was subjected to slight changes of a few mm for practical reasons related to different arrangements of ground 1 and ground 2 test by test.

$$h(n)_2 = \frac{1}{K_2 a^{2.5}} \frac{\psi(-n/a)_2}{\sqrt{a}}. \tag{6}$$

In Eq. (6) $\psi(n)$ corresponds to the Gaussian wavelet (Mallat, 2001; Gentile and Messina, 2003; Messina, 2004) related to the second derivative of the signal (Messina, 2004) and a is the dilation parameter to which the number of the filter points N_f: $N_f = 10 \cdot a + 1$ corresponds.

Before closing this introductory part of the present section it should be taken into account that due to the fact that all measurements started with the first point placed at about 44 mm (points) from the clamped section the damaged location in samples domain ($n = 1, \ldots, N$) can be found in all the subsequent graphs through the following equation:

$$n_c(samples) \approx Lc[mm] - 44, \tag{7}$$

where n_c represents the point identifying the centre of the notch in the samples domain along each single beam.

4.1. The sensitivity of the second derivative on the curvature and the ability of a fitting method in detecting damaged locations

In the case herein dealt with the crack was simulated by realizing three notches at $n_c \approx 57$, 160 and 260. Only the third notch is located, as established in Table 6, at the maximum curvature of the undamaged mode shape whilst the first two are located in the proximity of a zero curvature placed near the clamped end. This case clearly illustrates how the capability of the second derivative in detecting damage is modulated by the curvature of the system under test. In this respect, Figs. 10 and 11 should be taken into account. Both the above mentioned pictures are related to an experiment carried out over about 520 test points and show, looking from the top to the bottom, three graphs: the mode shape and its polynomial fit, the residual noise and, finally, the processing of the mode shape through its convolution with (6) and herein indicated as D_2 (to recall the second derivative of the processed dynamic shape). Figs. 10 and 11 are processed through a dilation parameter $a = 8$ (*i.e.*, Eq. 6) and $a = 12$, respectively. The order of the polynomial curve fitter was adopted coincident to the dilation parameters for all the numerical processing in the relevant figures.

As is discussed in Messina (2004) the convolving filter becomes longer as the dilation parameter increases and thus accomplishing a greater removal of noise. Both the phenomena are also shown inside the third graphs of Figs. 10 and 11. In these graphs an increasing black bold line indicates the length of the convolving filter (6); a greater removal of noise at higher dilation parameters is also clearly illustrated by comparing Figs. 10 and 11. The greater removal, however, also causes a smoothing of the peaks which are representative of the damaged locations ($n_c \approx 57$, 160, 260). This behaviour is explained in references (Gentile and Messina, 2003; Messina, 2004) and here it must be considered as a full experimental validation. It is finally interesting to notice that the highest peak occurs at the maximum curvature whilst the others, although characterized by an identical depth of the crack, are smaller and algebraically modulated by the curvature of the beam.

What is additionally interesting to notice in Figs. 10 and 11 is the capability of the polynomial fit (residual noise) in identifying the location of the notches; indeed, a cusp is clearly located at $n_c \approx 260$ and is strictly related to the damage placed in that location. Smaller damage cannot be clearly identified by the fitting in

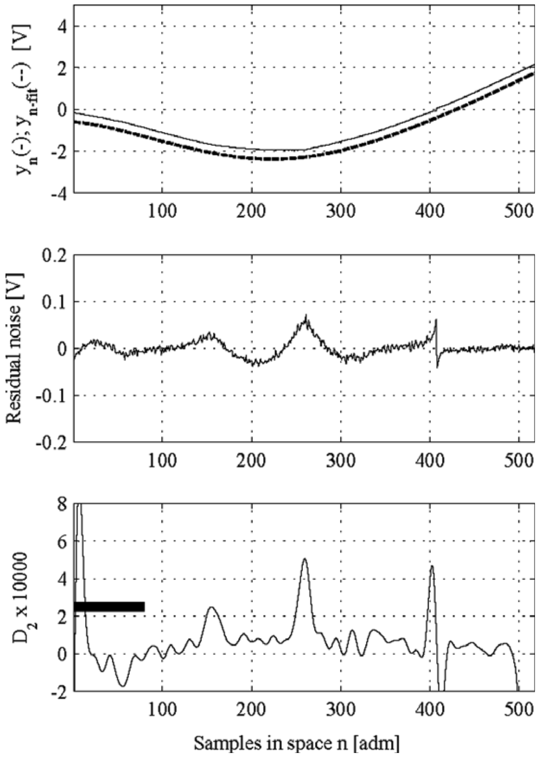

Fig. 10. Dynamic shape of beam2 containing 3 notches ($n_c = 57, 160, 260$). Shape measured, fitted ($p = 8$) and processed with Gaussian wavelet through dilation parameter $a = 8$.

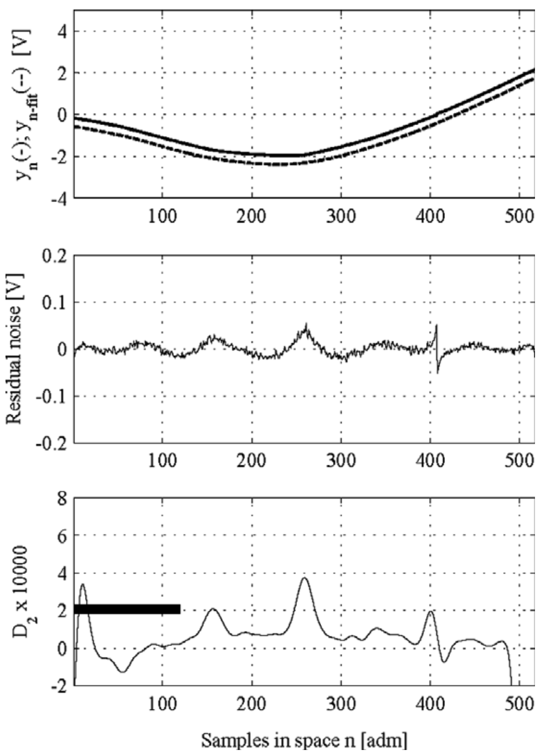

Fig. 11. Dynamic shape of beam2 containing 3 notches ($n_c = 57, 160, 260$). Shape measured, fitted ($p = 12$) and processed with Gaussian wavelet through dilation parameter $a = 12$.

so much as they are highlighted by the peaks through D_2. However, even though the fitting tool seems to be less obvious than D_2, it can assist in several situations and particularly at low value of dilation parameters where the noise can heavily mask the peaks whilst low orders of polynomial fitting are able to provide cusps in damaged locations. Moreover, the fitting method herein suggested should also be taken into account in order to provide the analyst with an idea concerning the amount of noise which is present in the measurements. Finally, the fitting procedure can also reveal outliers (*e.g.*, $n \approx 407$ in Figs. 10 and 11) which, whether are not appropriately identified, can cause false damage detections. These so-called outliers are those well known local measurement uncertainties (*e.g.*, Press et al., 1992, p. 659) that can occur in unknown circumstances and significantly deviate from a statistical distribution. In this respect, outliers cannot generally be excluded by an experimental procedure. However, because the present investigation is aimed at identifying local peaks as damage indicators there is the natural need to recover any information aimed at excluding or accepting a peak as true damage. In particular, the relevant outliers of Figs. 10 and 11 are due to the change of phase of the dynamical shape around the nodal point (*i.e.*, zero displacement) of the dynamical shape; a perusal at the experimental data (here not reported for the sake of brevity) revealed that this was simply due to the extremely low level of the signal along with the uncertainty to correlate with the phase of the accelerometer (Fig. 1). Rare outliers (*e.g.*, Fig. 8b, $n = \sim 430$) are also present without a clean explanation. The outliers due to a phase variation can be separately tackled; however, it is believed that all the mentioned outliers can be discerned from true damage by accompanying the continuous wavelet transform with a fitting procedure which also shows the amount of noise in the measurements; indeed the outliers are easily identified as an extremely located peak or abrupt change, therefore, profoundly different from a definitely milder cusp related to a stiffness change.

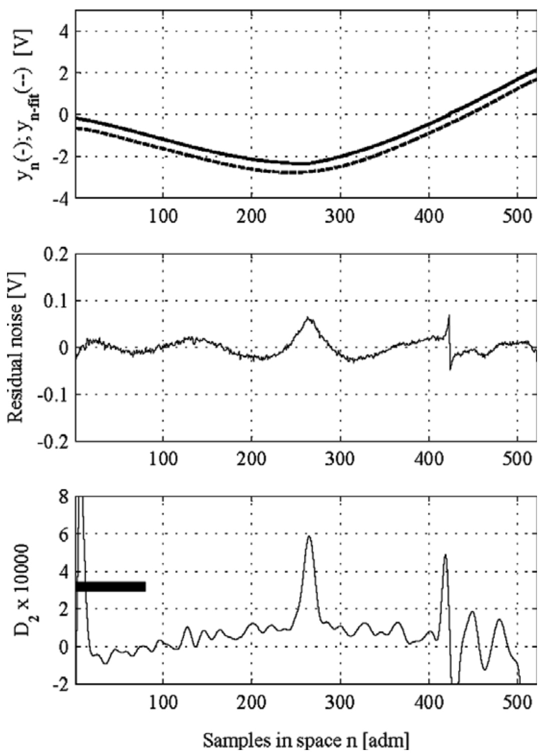

Fig. 12. Dynamic shape of beam2 (ref. Table 6). Shape measured, fitted ($p = 8$) and processed with Gaussian wavelet through dilation parameter $a = 8$.

4.2. On the influence of the thickness for detecting cracks

The experimental investigations illustrated in this subsection are not only aimed at showing the universality of the matters theoretically discussed in references (Gentile and Messina, 2003; Messina, 2004) (*i.e.*, providing relevant validation). These experimental investigations also show the effectiveness of certain differentiator filters in identifying damaged locations with respect to several beams. In particular, this section investigates a dependence of the technique on the specific beams under test. To this end all the following Figs. 12–19 are arranged identically to Figs. 10 and 11 as already mentioned above.

First of all, Figs. 12 and 13 should be compared to Figs. 14 and 15, respectively. The first ones are related to the thicker beam2 (ref. Tables 1 and 6) whilst the second ones describe the case of beam1. As Table 6 clearly indicates, beam1 and beam2 have approximately the same length identical crack depth but a remarkably different thickness (3.4 mm for beam1 and 16 mm for beam2). It is believed that the different time-sampling detail does not make any difference in the context. The comparisons of these figures clearly illustrate that in the case of the thicker beam (beam2) in Figs. 12 and 13 the indicator peak is clean and abundantly higher of the noise at the base; perhaps the damage can also be seen through a careful visual examination of the dynamic shape; above all, the damage in beam2 can certainly and also be seen through the cusp shown by the residual noise. The situation is less successful in the case of beam1. Indeed, Figs. 14 and 15 need a non-negligible amount of imagination of the analyst in order to identify a clean indicator peak above the noise at the base. In this case it should be considered that the amount of noise in the measurement of the dynamic shape in Fig. 14 and 15 was estimated to be 54 dB with a standard deviation of about 5 mV and a maximum displacement of 2.7 V (541 μm) at the end of the beam. In spite of such high signal/noise ratio the extraction of a 50%-damage (placed on the other hand in the most sensitive location of the mode shape) is unclear in Figs. 14 and 15 and, therefore, it is also indicative of an apparent undamaged beam. Another indicator of the absence of a

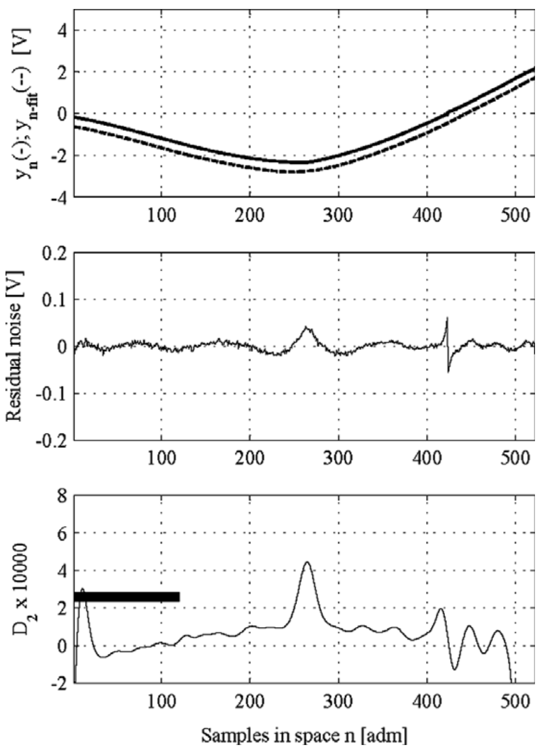

Fig. 13. Dynamic shape of beam2 (ref. Table 6). Shape measured, fitted ($p = 12$) and processed with Gaussian wavelet through dilation parameter $a = 12$.

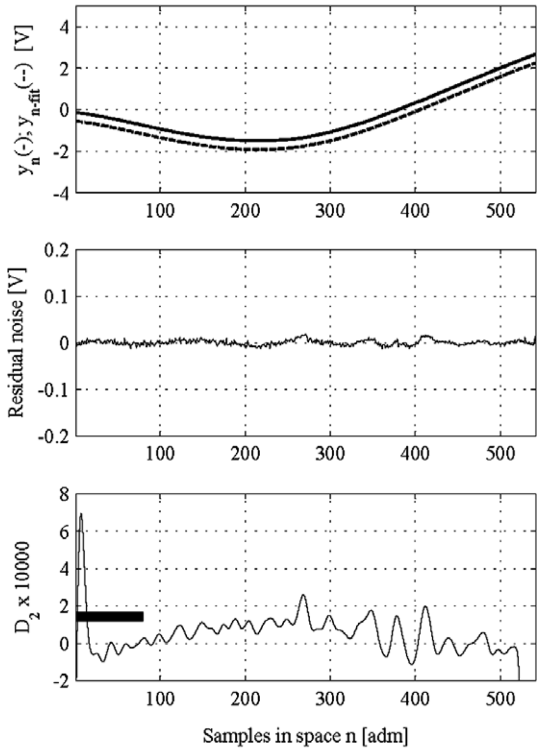

Fig. 14. Dynamic shape of beam1 (ref. Table 6). Shape measured, fitted ($p = 8$) and processed with Gaussian wavelet through dilation parameter $a = 8$.

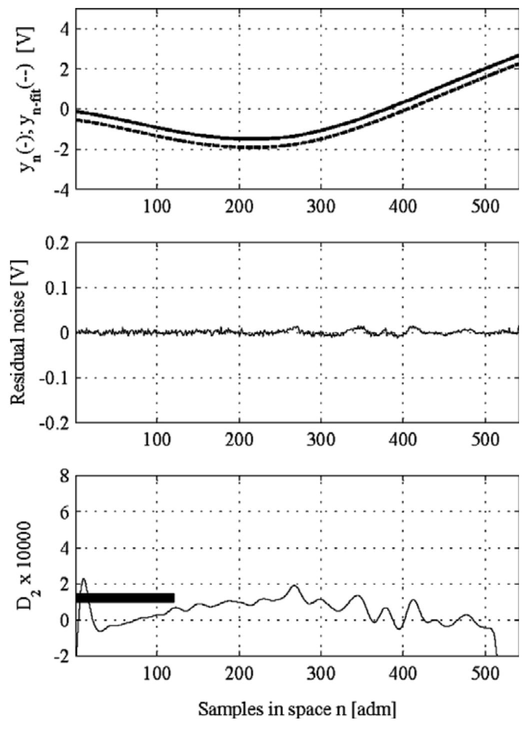

Fig. 15. Dynamic shape of beam1 (ref. Table 6). Shape measured, fitted ($p = 12$) and processed with Gaussian wavelet through dilation parameter $a = 12$.

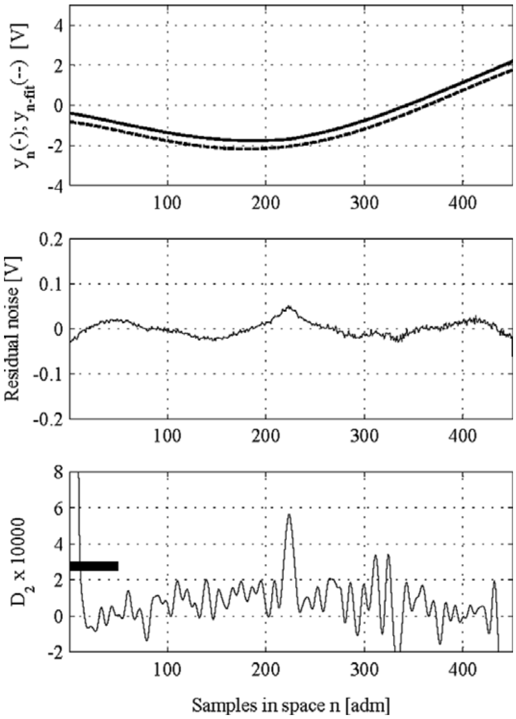

Fig. 16. Dynamic shape of beam3 (ref. Table 6). Shape measured, fitted ($p = 5$) and processed with Gaussian wavelet through dilation parameter $a = 5$.

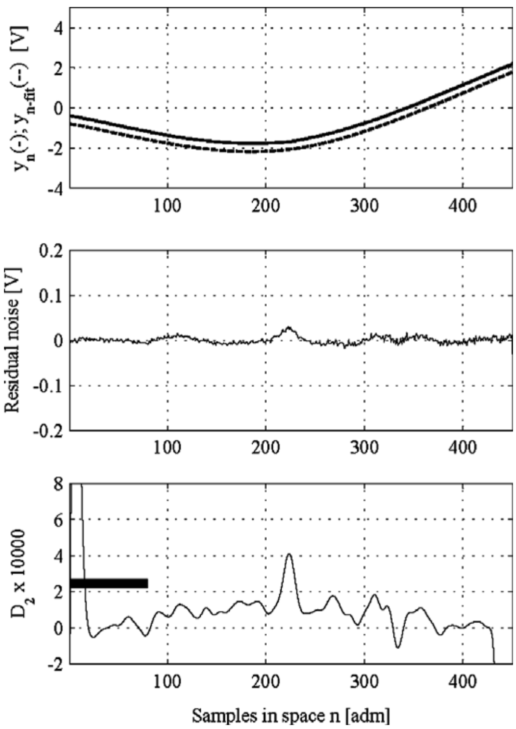

Fig. 17. Dynamic shape of beam3 (ref. Table 6). Shape measured, fitted ($p = 8$) and processed with Gaussian wavelet through dilation parameter $a = 8$.

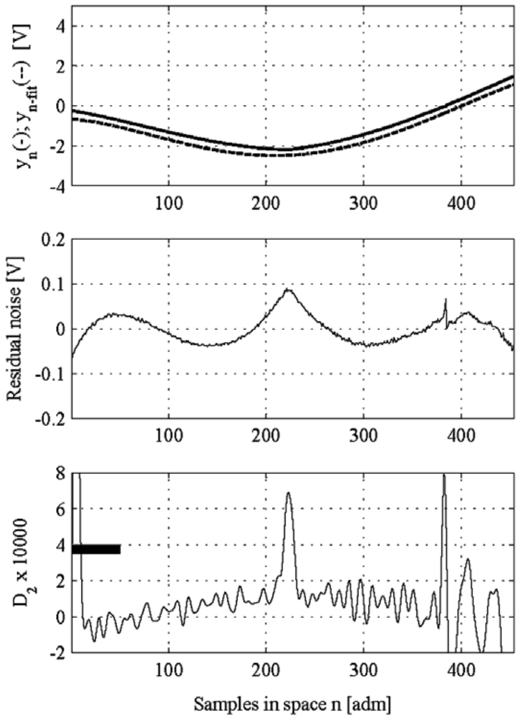

Fig. 18. Dynamic shape of beam4 (ref. Table 6). Shape measured, fitted ($p = 5$) and processed with Gaussian wavelet through dilation parameter $a = 5$.

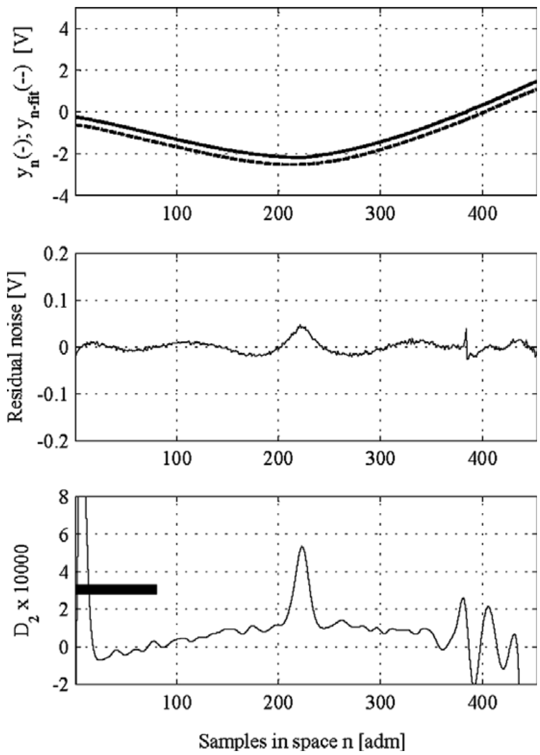

Fig. 19. Dynamic shape of beam4 (ref. Table 6). Shape measured, fitted ($p = 8$) and processed with Gaussian wavelet through dilation parameter $a = 8$.

damage is the drop in the signal/noise ratio due to the presence of cusps in the residual noise; such a drop that did not occur in beam1.

The experiment related to Figs. 12–15 highlights the remarkable influence of the thickness of a beam in the identification of a damage.

The conclusion that the thickness of a beam can influence the identification process has also been corroborated by the analysis carried out on beam3 and beam4. The relevant pictures concerning this case are Figs. 16 and 17 for beam3 and Figs. 18 and 19 for beam4. These beams, differently from beam1 and beam2, also have identical length (500 mm) and identical material (epoxy glass laminate); therefore, the thickness is the only difference (5 mm, 10 mm). Figs. 16 and 17 should be compared to Figs. 18 and 19, respectively. A perusal at these respective figures clearly confirms the influence of the thickness and of the noise in identifying damaged locations through the use of differentiator filters. Indeed, the indicator peaks are shown as depending on the thickness of each analyzed beam at fixed conditions for providing higher peaks for thicker beams.

This subsection basically settles the importance to investigate possible analytical tools aimed at simulating, in order to establish a priori, and case by case, the feasibility of the diagnosing technique over an established threshold of noise.

5. Conclusions and recommendations

In this work a thorough experimental investigation into the applicability of certain recently proposed mathematical tools such as certain continuous wavelet transforms has been conducted for damage detection purposes of open cracks in transversally vibrating beams.

An impressive experimental investigation, based on a huge number of tested points (~500, with a density of 1 point/mm) over several beams, has confirmed the numerical predictions that were conducted in the past (Gentile and Messina, 2003; Messina, 2004) thus validating the relevant results. This has been carried out by adopting an experimental technique, which, in spite of its own simplicity was able to provide dynamic shapes containing an extremely low amount of noise (signal/noise ratio slightly higher than 50 dB). In this regard it should be of interest to notice that usually mode shape extraction techniques bring displacement fields which usually contain errors whose standard deviation can even reach 10–30% of the maximum values of the mode shapes; therefore, the details concerning the experimental extracting technique should also be considered of a certain technical-scientific value. The simple technique adopted has thus allowed the application of differentiator numerical filters aimed at extracting useful diagnosing information for several dynamic shapes.

An accurate experimental error analysis, also based on circuits appropriately built for this research, has elucidated the successful or unsuccessful capability of the method to provide dynamic shapes with a high signal/noise ratio. The technique into account here is not expensive. However, the technique has the limitation of the transversal positioning (24 mm, ±2 mm) and that concerning the resolution of the measured displacements (1 μm) at higher frequencies. In this respect, there exist modern laser scanning vibrometers which can overcome the mentioned limitations but their costs are still prohibitive for many laboratories worldwide thus not allowing relevant open investigations.

Along with the above mentioned valuable objectives this manuscript has, therefore, provided the following conclusive items: to a certain extent the adopted wavelets are confirmed to be equivalent to the derivatives to which the merit to correctly identify the damaged locations intrinsically belongs. In the presence of noise the finest scales are not the best choice because the noise masks the peaks identifying damaged locations.

The sensitivity of the derivative of a mode shape is curvature modulated, therefore any available mode should be processed in order to avoid any shadow site along the beam.

A dynamic shape should generally be preferred to a static shape in order to avoid the presence of a severe amount of noise caused by surface irregularities or predefined non-expected deformed states. Conversely, the experimental set-up adopted along with the extracted dynamical shapes filters out such irregularities and can decisively improve the signal/noise ratio.

The minimum detectable amount of damage cannot only be indicated through the depth of a notch in the sense that the diagnosing technique should also be validated with respect to the specific structural system under test. Indeed, the present work has experimentally highlighted that the dependency on the thickness of the beam exists, *thus allowing the technique a better identification for thicker beams*. This last point illustrates the need to investigate possible analytical tools aimed at evaluating a priori, the feasibility of the diagnosing technique over an established admissible threshold of noise and for the specific structural systems under test; in this sense, the present work should also be intended as providing lowest bounds of detectable damage when a technique based on the processing of dynamical shapes, through continuous wavelet transforms or differentiator filters, is taken into account.

References

Chukwujekwu Okafor, A., Dutta, A., 2000. Structural damage detection in beams by wavelet transforms. Smart Material Structures 6, 906–917.

Dimarogonas, A.D., 1996. Vibration of cracked structures: a state of the art review. Engineering Fracture Mechanics 55, 831–857.

Doebling, S.W., Farrar, C.R., Prime, M.B., 1998. A summary review of vibration-based damage identification methods. The Shock and Vibration Digest 30, 91–105.

Ewins, D.J., 1992. Modal Testing: Theory and Practice. John Wiley and Sons Inc., New York.

Gentile, A., Messina, A., 2003. On the continuous wavelet transforms applied to discrete vibrational data for detecting open cracks in damaged beams. International Journal of Solids and Structures 40, 295–315.

Han, J.-G., Ren, W.-X., Sun, Z.-S., 2005. Wavelet packet based damage identification of beam structures. International Journal of Solid and Structures 42, 6610–6627.

Heylen, W., Lammens, S., Sas, P., 2003. Modal analysis theory and testing, Publication of Katholieke Universiteit Leuven—Departement Werktuigkunde, Celestijnenlaan 300B, B-3001 Heverlee, Belgium, ISBN 90-73802-61-X.

Kim, H., Melhem, H., 2004. Damage detection of structures by wavelet analysis. Engineering Structures 26, 347–362.

Kim, B.H., Park, T., Voyiadjis, G.Z., 2006. Damage estimation on beam-like structures using the multi-resolution analysis. International Journal of Solid and Structures 43, 4238–4257.

Mallat, S., 2001. A Wavelet Tour of Signal Processing. Academic Press, New York.

MEL Mikroelektronik GMBH, 2002. Measuring Systems M5, manual. Laser Sensor: M5L/4.

Messina, A., 2004. Detecting damage in beams through digital differentiator filters and continuous wavelet transforms. Journal of Sound and Vibration 272, 385–412.

Messina, A., 2005. Progetto, Realizzazione e Test di un filtro analogico passa banda con banda/guadagno variabile. Private Report No. D14 (in Italian).

Pai, P.F., Young, L.G., 2001. Damage detection of beams using deflection shapes. International Journal of Solid and Structure 38, 3161–3192.

Pandey, A.K., Biswas, M., Samman, M.M., 1991. Damage detection from changes in curvature mode shapes. Journal of Sound and Vibration 145, 321–332.

Press, W.H., Teukolsky, S.A., Vetterling, W.T., Flannery, B.P., 1992. Numerical Recipes in C, second ed. Cambridge University Press.

Rao, S.S., 1995. Mechanical Vibrations. Addison Wesley Publishing Company, New York.

Rucka, M., Wilde, K., 2006. Application of continuous wavelet transform in vibration based damage detection method for beams and plates. Journal of Sound and Vibration 297, 536–550.

Salawu, O.S., 1997. Detection of structural damage through changes in frequency: a review. Engineering Structures 19, 718–723.

Waldron, K., Ghoshal, A., Schulz, M.J., Sundaresan, M.J., Ferguson, F., Pai, P.F., Chung, J.H., 2002. Damage detection using finite element and laser operational deflection shapes. Finite Elements in Analysis and Design 38, 193–226.

Yuen, M.M.F., 1985. A numerical study of the eigenparameters of a damaged cantilever. Journal of Sound and Vibration 103, 301–310.